Wavelength and intensity dependence of recollision-enhanced multielectron effects in high-order harmonic generation

Paul M. Abanador,[1,*] François Mauger,[1] Kenneth Lopata,[2] Mette B. Gaarde,[1] and Kenneth J. Schafer[1]

[1]*Department of Physics and Astronomy, Louisiana State University, Baton Rouge, Louisiana 70803-4001, USA*
[2]*Department of Chemistry, Louisiana State University, Baton Rouge, Louisiana 70803-4001, USA*

Using a model molecular system (A_2) with two active electrons restricted to one dimension, we examine high-order harmonic generation (HHG) enhanced by rescattering. Our results show that even at intensities well below the single ionization saturation, harmonics generated from the cation (A_2^+) can be significantly enhanced due to the rescattering of the electron that is initially ionized. This two-electron effect is manifested by the appearance of a secondary plateau and cutoff in the HHG spectrum, extending beyond the predicted cutoff in the single active electron approximation. We use our molecular model to investigate the wavelength dependence of rescattering enhanced HHG, which was first reported in a model atomic system [I. Tikhomirov, T. Sato, and K. L. Ishikawa, Phys. Rev. Lett. **118**, 203202 (2017)]. We demonstrate that the HHG yield in the secondary cutoff is highly sensitive to the available electron rescattering energies as indicated by a dramatic scaling with respect to driving wavelength.

I. INTRODUCTION

The study of atoms and molecules interacting with intense laser pulses ($10^{13} - 10^{16}$ W/cm^2) has revealed fundamental processes, including high-order harmonic generation (HHG) [1–4], nonsequential double ionization (NSDI) [5–8], and above-threshold ionization (ATI) [9–11]. These processes are generally interpreted by a semiclassical (or recollision-based) model [12–14]. In this model the electron is first ionized from its ground state and then accelerated in the continuum by the oscillating field. This ionized electron can be driven back by the field and thus recollide with the cation. In the case of HHG, the recollision leads to the emission of a photon with energy $\Omega = I_p + E_r$. Here I_p is the ionization potential of the target atom or molecule and E_r is the electron rescattering energy. Neglecting the effect of the Coulomb potential, the semiclassical model predicts the cutoff energy for HHG to be $I_p + 3.2U_p$, where U_p is the ponderomotive energy. This expression for the semiclassical cutoff energy is linked to the maximal energy for the returning electron, $3.2U_p$. In quantum mechanical calculations, the HHG process is typically described within the single active electron (SAE) approximation, which ignores dynamical multielectron effects.

In contrast to HHG, NSDI is a process that is understood to be driven by multielectron effects that are beyond the SAE approximation [15,16]. Numerous studies have indicated that these nonsequential effects dominate in strong field double ionization below the saturation intensity for the first ionization, beyond which sequential effects start to dominate [17–20]. In addition to direct impact ionization, alternative routes to recollision-driven double ionization have been identified, such as recollision excitation with subsequent ionization (RESI) [21,22]. In the RESI mechanism, the electron that is left in the cation is first promoted to an excited state by exchanging energy with the returning electron (recollision excitation), and it can later be ionized when the field is close to a maximum (subsequent ionization). When the maximal energy of the returning electron is not sufficient to directly knock out the second electron from the cation, the RESI mechanism is expected to be the dominant channel. Other studies have also proposed a mechanism involving multiple recollisions as important in the NSDI process [23,24].

The incorporation of nonsequential effects in the interaction of atoms and molecules with strong fields remains computationally challenging, particularly for quantum mechanical models. In this paper we investigate multielectron rescattering effects in HHG beyond the SAE approximation. We provide numerical evidence for the enhancement of HHG due to nonsequential effects by solving the two-active-electron (TAE) time-dependent Schrödinger equation (TDSE). Using a one-dimensional (1D) molecular model, we identify the secondary plateaus and cutoffs in HHG spectra arising from the recollision dynamics of the first ionized electron, as also recently reported in a model atomic system [25]. These secondary plateaus and cutoffs in our TAE molecular model extend beyond the results calculated from its corresponding effective SAE model. We show that the efficiency of the recollision-enhanced HHG process is mainly dependent on the U_p scaling of return energies with respect to the laser intensity and wavelength λ. In particular, our results suggest that these two-electron recollision effects are reduced for longer driving wavelengths, which exhibit a dramatic scaling of λ^{-6} for the HHG yield in the secondary cutoff.

This paper is organized as follows. In Sec. II, we present the 1D molecular model that we have implemented and the numerical details for the calculated HHG spectra and their associated time-frequency profiles. In Sec. III, we discuss and analyze the time-frequency profiles of emission from the recollision-enhanced HHG process and the corresponding

---

*Corresponding author: pabana1@lsu.edu

wavelength and intensity dependence of the secondary cutoff yields. Finally, we give a summary of our results and some implications for experimental studies in Sec. IV. Atomic units are used throughout this paper unless otherwise stated.

II. THEORETICAL METHODS

Using a 1D molecular model (A_2) with two active electrons, we numerically solve the TDSE:

$$i \frac{\partial}{\partial t} \Psi(x_1, x_2, t) = \hat{H}(x_1, x_2, t) \Psi(x_1, x_2, t). \quad (1)$$

The Hamiltonian, in the length gauge and dipole approximation, is given by

$$\hat{H} = \sum_{k=1}^{2} \left[-\frac{1}{2} \frac{\partial^2}{\partial x_k^2} + V_{ne}(x_k) \right]$$
$$+ V_{ee}(x_1, x_2) + (x_1 + x_2) F(t), \quad (2)$$

where V_{ne} is the electron-nucleus potential, V_{ee} is the electron-electron potential, and $F(t)$ is the driving laser field. In our calculations a linearly polarized laser field $F(t) = F_0 f(t) \sin(\omega t)$ is applied, where F_0 and ω are the laser peak amplitude and frequency, respectively. The envelope $f(t)$ ramps up during the first two laser cycles ($\tau = 4\pi/\omega$) and remains constant afterwards:

$$f(t) = \begin{cases} 0, & t < 0, \\ \sin^2(\pi t/2\tau), & 0 \leqslant t \leqslant \tau, \\ 1, & t > \tau. \end{cases} \quad (3)$$

Note that the ponderomotive energy is defined as $U_p = F_0^2/4\omega^2$, which corresponds to a quadratic scaling with respect to the driving wavelength and a linear scaling for the intensity.

Using soft-Coulomb potentials [26], the electron-nucleus and electron-electron interactions are respectively written as

$$V_{ne}(x) = -\frac{Z}{\sqrt{\left(x + \frac{R}{2}\right)^2 + a_{ne}^2}} - \frac{Z}{\sqrt{\left(x - \frac{R}{2}\right)^2 + a_{ne}^2}} \quad (4)$$

and

$$V_{ee}(x_1, x_2) = \frac{1}{\sqrt{(x_1 - x_2)^2 + a_{ee}^2}}, \quad (5)$$

where Z is the effective charge, R is the separation distance between the nuclei, and a_{ne} and a_{ee} are the softening parameters. Here we assume that the positions of the nuclei are fixed during the temporal evolution. For the 1D A_2 molecular system, we set the parameters $Z = 1$, $R = 1.9$ a.u., $a_{ne}^2 = 0.7$, and $a_{ee}^2 = 1$. This results in the ionization potentials of A_2 and its cation A_2^+ to be $I_p^{(1)} = 21.1$ eV and $I_p^{(2)} = 38.9$ eV, respectively. The difference between the ionization potentials for the first and second electron can be controlled by varying the parameter R.

Numerical simulations presented in this work are implemented using the grid-based quantum code, OCTOPUS [27]. The initial state used in solving the TDSE is the ground state of the molecular system for both neutral and cationic species. In the neutral case, we solve the full TDSE for two active electrons, which hereafter is referred to as the A_2 TAE model. On the other hand, in the cationic case the TDSE is solved for effectively only one electron (A_2^+ SAE model).

For the A_2 TAE calculations, converged results are achieved with grid spacing $\Delta x = 0.4$ a.u. (in both electron coordinates) and time step $\Delta t = 0.03$ a.u. In all calculations we ensure that the noise level, e.g., due to spurious reflections from the applied absorbing boundaries, is much lower than the signal from secondary cutoffs in the HHG spectra.

Single-active-electron simulations are also employed in order to compare with TAE results and to identify two-electron effects present in our A_2 molecular model. In the SAE approximation, the dynamics is described by a single-electron wave function $\psi(x, t)$ such that

$$i \frac{\partial}{\partial t} \psi(x, t) = \hat{H}_{eff}(x, t) \psi(x, t)$$
$$= \left[-\frac{1}{2} \frac{\partial^2}{\partial x^2} + V_{eff}(x) + x F(t) \right] \psi(x, t). \quad (6)$$

In our study the effective potential $V_{eff}(x)$ is taken to have the same form as Eq. (4) with parameters changed to $Z = 0.5$ and $a_{ne}^2 = 0.4235$ to match the ionization potential of the two-electron A_2 molecular system.

The associated HHG spectrum is evaluated from the Fourier transform of the dipole acceleration $a(t)$ [28]. Throughout the paper we take the Fourier transform over the time duration of laser cycles 3–8, wherein a Hanning window is applied. For the time-frequency analysis we utilize the Gabor transform [29] as defined by

$$a_G(\Omega, t) = \int dt' a(t') \frac{\exp\left[-(t' - t)^2/2\sigma^2\right]}{\sigma \sqrt{2\pi}} \exp\left(-i\Omega t'\right), \quad (7)$$

where the standard deviation for the Gaussian window function is set as $\sigma = 1/(4\omega)$ or about 4% of the laser cycle.

III. RESULTS AND DISCUSSION

In this section we explore recollision-enhanced multielectron effects in HHG from the solution of the TDSE for two active electrons restricted to 1D. First, we consider the case of laser wavelength equal to 1400 nm and peak intensity equal to 5×10^{13} W/cm^2, which is well below the saturation intensity for the first ionization. Figure 1 shows that the HHG spectrum calculated from the A_2 TAE molecular model (solid red) has a primary cutoff at about 55 eV, which closely matches the cutoff energy from the SAE molecular model (dashed blue). This is consistent with the commonly used SAE semiclassical model which estimates the cutoff energy to be $I_p^{(1)} + 3.2U_p$ (≈ 50 eV). The discrepancy between actual and estimated values can be attributed to the additional kinetic energy acquired by the electron during recombination with the cation [14].

Aside from the primary cutoff that closely matches the A_2 SAE model shown in Fig. 1, the HHG spectrum for the A_2 TAE model also has a secondary cutoff at about 72 eV. The position of this second cutoff is in good agreement with the cutoff energy from the HHG spectrum for the A_2^+ SAE model (dotted green). This indicates that the corresponding secondary plateau is due to the contribution from HHG in the A_2^+ cation. Although the position of the secondary cutoff matches the SAE prediction for the cation, the strength of the secondary plateau is very different. We find an overall enhancement of
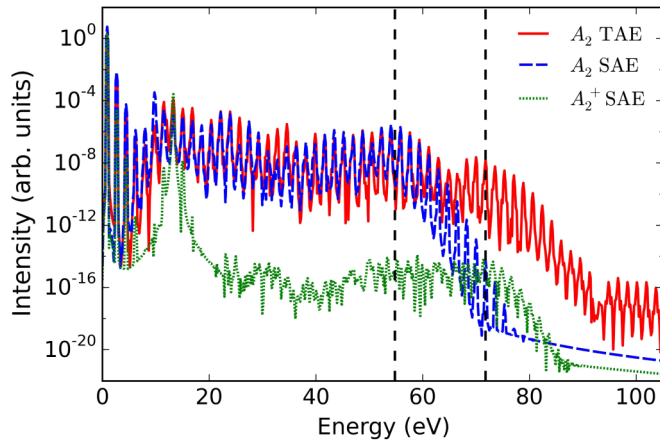
FIG. 1. HHG spectra generated from the A_2 TAE (solid red) and SAE (dashed blue) molecule and from its corresponding cation A_2^+ (dotted green). Here the driving laser field has a peak intensity of 5×10^{13} W/cm^2 and a wavelength of 1400 nm. For each system the simulation is initialized from its ground state. The vertical dashed lines correspond to the first and second cutoffs.

several orders of magnitude in the HHG yield at the secondary plateau for the A_2 TAE system compared to the A_2^+ SAE model. We note that the efficiency of the HHG process starting from the cation is predominantly determined by the ionization probability of the cation, and therefore can be associated to a sequential double ionization process. The fact that we find such a large enhancement of HHG from the cation when starting from the TAE neutral molecule suggests that the correlation between the rescattering electron and the remaining electron in the cation plays an important role. This is similar to the well known enhancement of NSDI dominating over sequential double ionization. In what follows we further substantiate these multielectron recollision effects.

The underlying mechanisms behind double ionization have been investigated in great detail using classical methods [30–32]. Briefly, in the RESI mechanism the first electron is ionized and driven back by the oscillating field. The initially ionized electron recollides with the cation and thus potentially exchanges energy with the second electron left in the cation. Depending on the energy exchange between the two electrons, the cation may be promoted to an excited state. This, in turn, enhances the second ionization and correspondingly the HHG in the cation. For the laser parameters considered in Fig. 1, the available energies of returning trajectories are comparable to the first excitation energy of A_2^+ (13.3 eV). Based on the investigation of classical double ionization, this condition has been shown to result in an efficient exchange of energy between the two electrons during recollision [33]. In the present work we are interested in how multielectron rescattering effects can be manifested in HHG spectra. We will present more evidence for the nonsequential mechanism behind the enhancement of HHG as well as examine its efficiency in the following.

A. Gabor analysis

We investigate the time-frequency profiles of the HHG emission using the Gabor analysis given in Eq. (7). This provides a way to visualize the emission times as well as the

relative yields of harmonics, particularly at the first and second cutoff energies. Figure 2 presents a comparison between the time-frequency profiles of the HHG emission for the two A_2 molecular models: (a) TAE and (b) SAE. As shown in Fig. 1, the position of the first cutoff is consistent for both models. For the time-frequency profile from the SAE model, there is no visible emission of harmonics beyond the first cutoff. However, emission in the secondary plateau can be clearly seen from the time-frequency profile for the TAE case.

As exhibited in Fig. 2(a), the harmonics in the first cutoff are emitted with nearly constant yield starting at the first half-cycle after the driving field ramp-up. We note that the time it takes for the harmonics in the secondary plateau to reach their full value is delayed by several half-cycles relative to the harmonics in the first cutoff (HHG in the neutral molecule). The delay in the harmonic emission supports the recollision-enhanced mechanism for the HHG in the cation, which is only initiated when the first electron that is ionized recombines with the cation. This is also in agreement with the time-frequency analysis from Ref. [25]. The enhancement in the secondary plateau relative to the A_2 SAE model is demonstrated by comparing the two panels of Fig. 2. This enhancement for the TAE model appears already starting at $t = 2.45$ laser cycles.

In addition to harmonic emission in the secondary plateau, we find remarkable differences in the structures from the TAE and SAE time-frequency profiles in Figs. 2(a) and 2(b) all through the primary plateau. These differences highlight the role of recollision effects in the HHG process. In particular, the enhancement of HHG from the A_2^+ cation in the TAE case appears to modify the overall shape of the time-frequency profile around the first cutoff (at 55 eV) when compared to the SAE case. In other words, near the primary cutoff the contributions from HHG in both the neutral and cationic species overlap, thereby resulting in the observed interference structures. At lower energies in the primary plateau, we see even more complicated structures for the TAE case shown in Fig. 2(a). The overlapping structures in the time-frequency profile make it somewhat difficult to distinguish contributions from different trajectories, e.g., the so-called short and long trajectories [34].

Next, we investigate how the signature of two-electron recollision effects in the HHG process is influenced by the laser wavelength. Figure 3 displays TAE and SAE time-frequency profiles for harmonics generated by a 2750 nm laser field with the same intensity as in Fig. 2. This increase in the wavelength corresponds to about four times higher U_p than the previous case. In Fig. 3(a), we indicate the emission of harmonics in the secondary plateau from the TAE model (white arrows). As expected from the recollision model of HHG, the position of the second cutoff relative to the first cutoff does not scale with the driving wavelength. Rather, the relative position of the second cutoff is determined only by the difference in ionization potentials, $I_p^{(2)} - I_p^{(1)}$. When compared to the case with shorter wavelength shown in Fig. 2(a), we observe the following from the time-frequency profile in Fig. 3(a). First, the second plateau has a much weaker relative yield in the case with longer wavelength. In addition, the emission of second-cutoff harmonics only appears starting at $t = 3.45$ laser cycles in Fig. 3(a). This means that the appearance of second-cutoff harmonics happens at later times in the case with longer
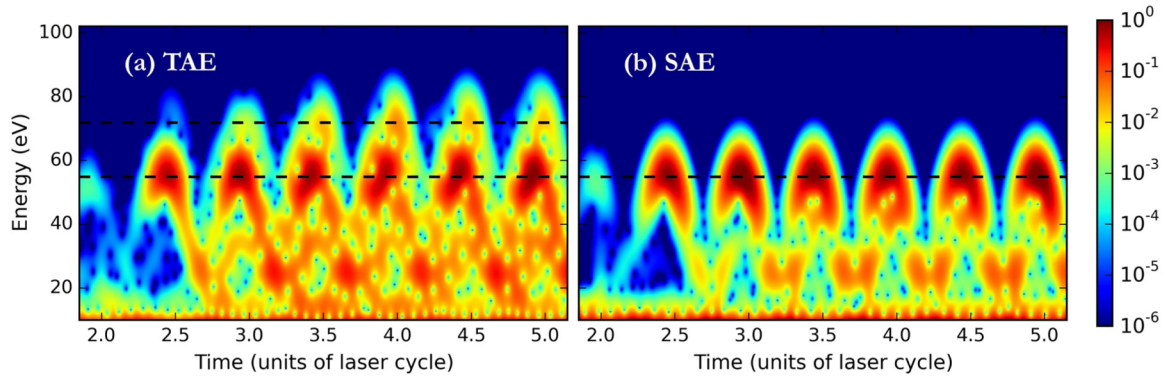
FIG. 2. Gabor analysis of the HHG from A_2 molecule with the same laser parameters as in Fig. 1. The time-frequency profiles are obtained from (a) TAE and (b) SAE simulations. The horizontal dashed lines correspond to the first and second cutoffs (same as previous figure). Only the first cutoff is indicated in (b).

wavelength. We also note that, in general, the TAE and SAE time-frequency profiles are much more similar in the longer wavelength case.

Additionally, we analyze the time profiles of harmonic emission near the two cutoff energies, which are displayed in Fig. 4. These time profiles correspond to horizontal lineouts from the Gabor mappings in Figs. 2(a) and 3(a). To be precise, the time profiles are Gabor transforms [given by Eq. (7)] evaluated at specific energies. Shown in the upper and lower panels of Fig. 4 are the time profiles for the two respective wavelengths, 1400 and 2750 nm. In the case of shorter wavelength, the time profile for the first cutoff in the TAE case (solid blue) shows that the yield levels off starting at $t = 2.45$ laser cycles, within the first half-cycle after the ramp-up. On the other hand, the second cutoff (dotted red) gradually increases and then levels off roughly at $t = 3.45$ laser cycles, which is delayed by a full cycle compared to the first cutoff. This reflects the delayed emission from the secondary cutoff that is visible in Fig. 2(a). Compared to the primary cutoff, harmonics in the secondary cutoff are generated from an additional recollision of the second electron, which has been initially ionized by the recollision of the first electron. In the case of the second-cutoff harmonics, the second electron has to travel in the continuum for about 2/3 of a laser cycle after being ionized from the cation. The travel time of the second

electron explains why the observed delay in the emission of second-cutoff harmonics is more than a half-cycle. In the same way, it means that the residual second-cutoff yields observed before $t = 3.45$ laser cycles are due to recollisions of the first electron during the ramp-up of the laser field.

As we have previously discussed, modifications in the time-frequency profile are observed for the shorter wavelength case, particularly near the first cutoff energy. From the time profiles in the upper panel of Fig. 4, we find the corresponding HHG emission peaks that are recurring every half-cycle after the ramp-up for both the first and second cutoffs. These peaks are in generally good agreement with the semiclassical prediction (vertical gray lines), which is about 0.05 laser cycle before zeros of the field. However, we note that the peaks for the first (second) cutoff are slightly shifted to earlier (later) times compared to the semiclassical prediction, starting at $t = 3.45$ laser cycles. This corresponds to the same time when the yield in the second cutoff levels off, indicating that the HHG from the A_2^+ cation has gained sufficiently high yield for it to interfere with the HHG from the A_2 molecule. Our results suggest that this leads to a slight preference for the short trajectory near the first cutoff region and a slight preference for the long trajectory near the second cutoff region, which can also be seen from Fig. 2(a). As a reference, the time profiles for the first cutoff from the SAE model (dashed cyan) are also shown in both
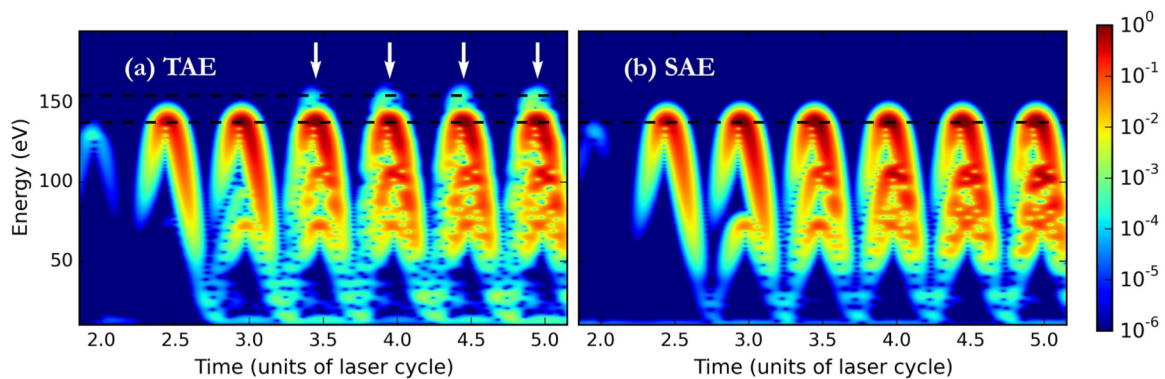

FIG. 3. Gabor analysis of the HHG from A_2 molecule with the same laser peak intensity as in Fig. 2 but with a different wavelength, 2750 nm. The horizontal dashed lines for the first and second cutoffs are shown, similar to Fig. 2. The white arrows indicate emission at the second cutoff present in (a) TAE simulation but not in (b) SAE simulation.
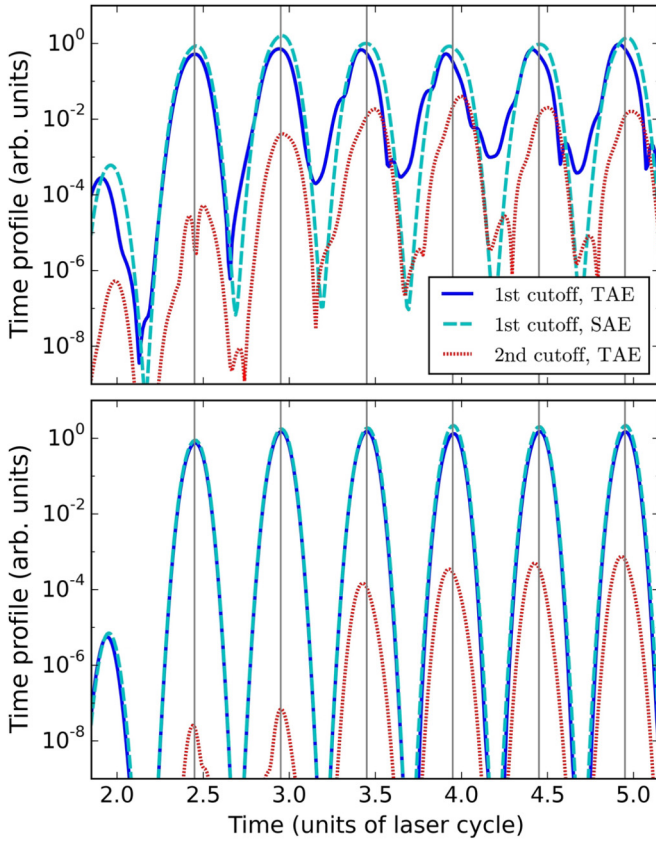
FIG. 4. Time profiles of the first (solid blue) and second (dotted red) cutoffs from TAE calculations. As a reference, the time profiles of the first cutoff (dashed cyan) from SAE calculations are also shown. The upper and lower panels correspond to driving field wavelengths of 1400 and 2750 nm, respectively, from the previous figures. The vertical gray lines indicate emission times predicted by the semiclassical model.

panels of Fig. 4. For the SAE case, peaks in the time profiles of the first cutoff are nearly mirror-symmetric and centered at emission times close to the semiclassical prediction.

Next, we inspect the time profiles from the longer wavelength case displayed in the lower panel of Fig. 4 and compare them with the shorter wavelength case. Although emission of second-cutoff harmonics is still observed in the case of longer wavelength, the relative HHG yield for the second cutoff is much lower compared to the case of shorter wavelength. Additionally, instead of a gradual increase, the yield for the second cutoff suddenly increases from $t = 2.95$ to 3.45 laser cycles and remains almost constant thereafter. We attribute this difference for the two wavelengths to the recollisions during the ramp-up. The gradual increase in the second-cutoff HHG yield for the shorter wavelength case shows that recollisions during the ramp-up can lead to enhancement in the subsequent half-cycles. For the longer wavelength case, there is almost no enhancement of the second-cutoff HHG yield during the first cycle after ramp-up, which means that recollisions during the ramp-up have very little effect. We find that the second-cutoff yields associated to recollisions during the ramp-up are relatively sensitive to its duration. Nevertheless, we find robust and consistent results for later times, one laser cycle after the

ramp-up, when the second-cutoff yields have plateaued and the associated laser peak intensity is well defined. These later times are of interest in our analysis here and we therefore focus on them in the remainder of the paper.

In general, we observe that the HHG spectra for SAE calculations become closer to the corresponding TAE results when the wavelength is increased. For instance, notice that time profiles at the first cutoff from TAE and SAE models are in almost perfect agreement for the longer wavelength case, which is illustrated in the lower panel of Fig. 4. This is expected since there is overall a very good agreement in the time-frequency profiles from the TAE and SAE models, as demonstrated in Fig. 3 (except for the emission at the secondary cutoff). The agreement between the two models suggests that the recollision-enhanced HHG process is suppressed for the longer wavelength case and that HHG from the neutral molecule dominates over HHG from the cation. Hence the recollision mechanism is not as efficient in enhancing HHG yields from the cation in the high U_p limit. In some sense, this justifies the use of SAE models in this regime where two-electron recollision effects are diminished. Improvement in the performance of SAE models for longer wavelengths has also been discussed and studied for ATI using the same two-electron model [35].

B. Wavelength and intensity dependence

For a more comprehensive analysis of the wavelength dependence, we calculate the HHG yields at the two cutoffs for varying wavelengths from 1000 to 3000 nm using the TAE A_2 model (see Fig. 5). Aside from fluctuations presumably due to channel closings [36,37], the relative HHG yield for the second cutoff decreases drastically with increasing wavelength. Here we evaluate the efficiency for the recollision-enhanced HHG by comparing the trends in the yields for the first and second cutoffs, labeled Y_{C1} and Y_{C2}. These yields, which are directly
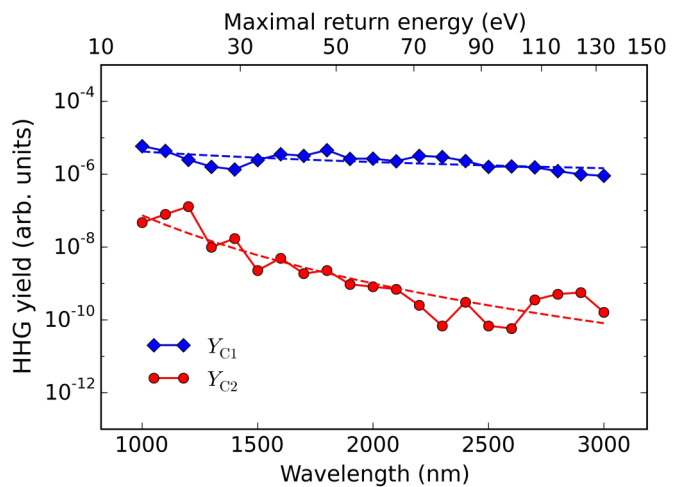

FIG. 5. Wavelength dependence of the yields at the first and second cutoffs obtained from TAE calculations, indicated by diamonds (Y_{C1}) and circles (Y_{C2}). The fitted trends (dashed curves) are also shown with λ^{-1} and λ^{-6} dependence for Y_{C1} and Y_{C2}, respectively. The peak intensity is fixed at 5×10^{13} W/cm^2. The scale for corresponding maximal return energies, $3.2U_p$, is included.
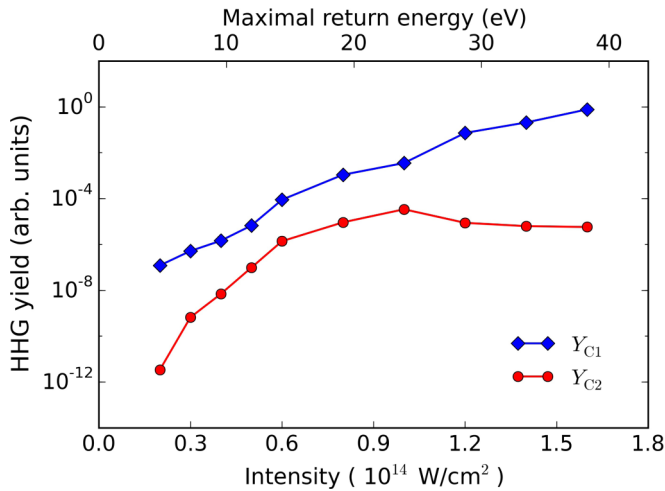
FIG. 6. Intensity dependence of the yields at the first and second cutoffs obtained from TAE calculations, indicated by diamonds (Y_{C1}) and circles (Y_{C2}). The driving wavelength is fixed at 900 nm. As in Fig. 5, the scale for corresponding maximal return energies is included.

obtained from the HHG spectra, are defined as the values of the HHG intensities at the respective cutoff harmonics. The overall scaling of the yield with driving wavelength is about λ^{-1} for the first cutoff while the scaling for the second cutoff is about λ^{-6}. To explain the difference in the wavelength scalings for the first- and second-cutoff yields, we compare the mechanisms responsible for the HHG emission, i.e., an additional recollision event for the second cutoff. In the subsequent dynamics following ionization, these mechanisms for HHG in both the neutral molecule and the cation is essentially the same and therefore we expect a similar wavelength scaling of λ^{-1} due to the spreading of the wave packet in 1D. Thus the remaining factor in the scaling of the second-cutoff yields that is from the recollision enhancement is equal to λ^{-5}. This can be further separated into two components: (1) the electron wave packet recolliding with the cation and (2) the efficiency of the recollision for enhancing the second ionization [38]. The former component simply gives another factor of λ^{-1} from the wave packet spreading. Consequently, the latter factor is equal to λ^{-4}, which is attributed to the efficiency for the ionization enhancement. Such a dramatic scaling is consistent with the analysis of energy exchange in classical NSDI studies [39]. Physically, this means that increasing the energy available from the returning electron results in a decline in efficiency. The resulting wavelength scaling indicates that the two-electron enhancement effects in HHG may be limited in the regime of relatively long wavelengths, specifically when the maximum return energies are higher than the second ionization potential.

From the limitation related to the wavelength scaling, a natural question that arises is whether there is an optimal U_p for the recollision-enhanced mechanism as reflected in calculated HHG spectra. Hence we discuss how the U_p scaling for increasing laser intensity affects the recollision-enhanced HHG process when the wavelength is fixed. In Fig. 6, we show the trends in the intensity dependence of HHG yields from the first and second cutoffs for a wavelength of 900 nm. Using this wavelength allows us to increase the intensity such that the

corresponding U_p's are similar to the shorter wavelengths from Fig. 5. As illustrated from the intensity dependence in Fig. 6, the rates by which both first- and second-cutoff HHG yields increase are roughly the same for the intermediate intensities, 0.5–1.0×10^{14} W/cm^2. In this regime the corresponding return energies, which are determined by U_p, are comparable to the first excitation energy of A_2^+ (13.3 eV). Overall, this range of laser intensities results in a relatively high efficiency for the enhancement of HHG in the second cutoff compared to the lower intensities. For the lowest intensity considered in Fig. 6, Y_{C2} is very low (4–5 orders of magnitude lower than Y_{C1}) since the return energy is hardly sufficient to excite the cation. Interestingly, we note that the ratio Y_{C2}/Y_{C1} within the intermediate intensity range is almost unaffected by the increase in intensity.

Increasing the driving intensity further brings us into the regime wherein the available return energies become closer to the second ionization potential. As discussed in the wavelength dependence, the increase in return energies does not necessarily translate into improved efficiency for the recollision-enhanced HHG process. In fact, the resulting efficiency is demonstrated to turn over as the intensity is increased above 1.0×10^{14} W/cm^2 in Fig. 6 [40]. We find that the second-cutoff yield remains almost constant while the first-cutoff yield increases; thus the ratio Y_{C2}/Y_{C1} decreases with increasing intensity. Again, this is consistent with the analysis of NSDI trends with respect to the laser intensity using a classical model [39]. In our analysis, we have similarly exhibited an optimal condition for the enhancement of HHG from secondary cutoffs based on the U_p scaling of electron rescattering energies for increasing intensity.

Altogether, the trends we find indicate that the decrease in efficiency for the HHG in the cation is mainly due to the scaling of rescattering energies as determined by U_p. These results are consistent with our proposed mechanism for the recollision-enhanced HHG process. Although the spreading of the electron wave packet can play a critical role in the wavelength scaling of NSDI [41], this factor has negligible effect in our 1D model. By calculating the ratio Y_{C2}/Y_{C1} with increasing wavelength while U_p is fixed, the ratio between the yields is found to be nearly independent of λ for the range of intermediate intensities considered in Fig. 6. Therefore, the wave packet spreading does not significantly contribute to the wavelength dependence of relative HHG yield for the secondary cutoff.

IV. SUMMARY AND CONCLUSIONS

In summary, we have investigated the role of nonsequential dynamics in the HHG process for multielectron systems using a 1D A_2 molecular model. From the solution of the two-electron TDSE, recollision effects are shown to give rise to the enhancement of HHG in the A_2^+ cation. This enhancement is manifested by the secondary plateaus and cutoffs in the HHG spectra, which extend beyond the commonly used SAE approximation. In particular, the recollision-enhanced HHG is observed to be most pronounced at intensities below the saturation of the first ionization such that effects related to NSDI become important. By applying Gabor analysis, we provide evidence for a nonsequential mechanism for the HHG in the cation. We find that the emission of second-cutoff

harmonics can be delayed by a full laser cycle compared to the first-cutoff harmonics. In addition, our results indicate that the efficiency of this recollision-enhanced HHG process is mainly dependent on the U_p scaling of the electron rescattering energies. We determine a dramatic scaling of λ^{-6} for the HHG yield in the second cutoff, thereby suggesting that the two-electron recollision effects are diminished for longer driving wavelengths. This, in turn, results in the improvement of the performance of SAE models for calculating HHG spectra in this high U_p regime.

Experimental observations of the secondary cutoffs in HHG spectra investigated here seem to be accessible with current or near-future technology. For example, recent measurements have characterized the contribution from the second least bound orbital (HOMO-1) of N_2 in the cutoff region of HHG

spectra [42]. In our study we provide insights for the design of experiments that can capture signatures of multielectron rescattering effects in HHG. Generally speaking, atoms and molecules with a difference between the first and second ionization potentials, which can be spectrally separated, are the best candidates for such experiments.

ACKNOWLEDGMENTS

[1] A. McPherson, G. Gibson, H. Jara, U. Johann, T. S. Luk, I. A. McIntyre, K. Boyer, and C. K. Rhodes, J. Opt. Soc. Am. B **4**, 595 (1987).

[2] M. Ferray, A. L'Huillier, X. F. Li, L. A. Lompre, G. Mainfray, and C. Manus, J. Phys. B **21**, L31 (1988).

[3] A. D. Bandrauk and H. Lu, J. Phys. B **38**, 2529 (2005).

[4] Y. P. Li, S. J. Yu, X. Y. Duan, Y. Z. Shi, and Y. J. Chen, J. Phys. B **49**, 075603 (2016).

[5] J. B. Watson, A. Sanpera, D. G. Lappas, P. L. Knight, and K. Burnett, Phys. Rev. Lett. **78**, 1884 (1997).

[6] S. Larochelle, A. Talebpour, and S. L. Chin, J. Phys. B **31**, 1201 (1998).

[7] C. Ruiz, L. Plaja, L. Roso, and A. Becker, Phys. Rev. Lett. **96**, 053001 (2006).

[8] B. Bergues, M. Kübel, N. G. Johnson, B. Fischer, N. Camus, K. J. Betsch, O. Herrwerth, A. Senftleben, A. M. Sayler, T. Rathje, T. Pfeifer, I. Ben-Itzhak, R. R. Jones, G. G. Paulus, F. Krausz, R. Moshammer, J. Ullrich, and M. F. Kling, Nat. Commun. **3**, 813 (2012).

[9] P. Kruit, J. Kimman, H. G. Muller, and M. J. van der Wiel, Phys. Rev. A **28**, 248 (1983).

[10] G. G. Paulus, W. Nicklich, H. Xu, P. Lambropoulos, and H. Walther, Phys. Rev. Lett. **72**, 2851 (1994).

[11] J. S. Parker, L. R. Moore, K. J. Meharg, D. Dundas, and K. T. Taylor, J. Phys. B **34**, L69 (2001).

[12] K. J. Schafer, B. Yang, L. F. DiMauro, and K. C. Kulander, Phys. Rev. Lett. **70**, 1599 (1993).

[13] P. B. Corkum, Phys. Rev. Lett. **71**, 1994 (1993).

[14] M. Lewenstein, P. Balcou, M. Y. Ivanov, A. L'Huillier, and P. B. Corkum, Phys. Rev. A **49**, 2117 (1994).

[15] C. Figueira de Morisson Faria and X. Liu, J. Mod. Opt. **58**, 1076 (2011).

[16] W. Becker, X. Liu, P. J. Ho, and J. H. Eberly, Rev. Mod. Phys. **84**, 1011 (2012).

[17] A. l'Huillier, L. A. Lompre, G. Mainfray, and C. Manus, Phys. Rev. A **27**, 2503 (1983).

[18] D. N. Fittinghoff, P. R. Bolton, B. Chang, and K. C. Kulander, Phys. Rev. Lett. **69**, 2642 (1992).

[19] B. Walker, B. Sheehy, L. F. DiMauro, P. Agostini, K. J. Schafer, and K. C. Kulander, Phys. Rev. Lett. **73**, 1227 (1994).

[20] M. G. Pullen, B. Wolter, X. Wang, X.-M. Tong, M. Sclafani, M. Baudisch, H. Pires, C. D. Schröter, J. Ullrich, T. Pfeifer,

R. Moshammer, J. H. Eberly, and J. Biegert, Phys. Rev. A **96**, 033401 (2017).

[21] B. Feuerstein, R. Moshammer, D. Fischer, A. Dorn, C. D. Schröter, J. Deipenwisch, J. R. Crespo Lopez-Urrutia, C. Höhr, P. Neumayer, J. Ullrich, H. Rottke, C. Trump, M. Wittmann, G. Korn, and W. Sandner, Phys. Rev. Lett. **87**, 043003 (2001).

[22] A. Rudenko, K. Zrost, B. Feuerstein, V. L. B. de Jesus, C. D. Schröter, R. Moshammer, and J. Ullrich, Phys. Rev. Lett. **93**, 253001 (2004).

[23] P. J. Ho, R. Panfili, S. L. Haan, and J. H. Eberly, Phys. Rev. Lett. **94**, 093002 (2005).

[24] Y. Liu, S. Tschuch, A. Rudenko, M. Dürr, M. Siegel, U. Morgner, R. Moshammer, and J. Ullrich, Phys. Rev. Lett. **101**, 053001 (2008).

[25] I. Tikhomirov, T. Sato, and K. L. Ishikawa, Phys. Rev. Lett. **118**, 203202 (2017).

[26] J. Javanainen, J. H. Eberly, and Q. Su, Phys. Rev. A **38**, 3430 (1988).

[27] X. Andrade, D. Strubbe, U. De Giovannini, A. H. Larsen, M. J. T. Oliveira, J. Alberdi-Rodriguez, A. Varas, I. Theophilou, N. Helbig, M. J. Verstraete, L. Stella, F. Nogueira, A. Aspuru-Guzik, A. Castro, M. A. L. Marques, and A. Rubio, Phys. Chem. Chem. Phys. **17**, 31371 (2015).

[28] K. Burnett, V. C. Reed, J. Cooper, and P. L. Knight, Phys. Rev. A **45**, 3347 (1992).

[29] C. C. Chirilă, I. Dreissigacker, E. V. van der Zwan, and M. Lein, Phys. Rev. A **81**, 033412 (2010).

[30] Y.-B. Li, X. Wang, B.-H. Yu, Q.-B. Tang, G.-H. Wang, and J.-G. Wan, Sci. Rep. **6**, 37413 (2016).

[31] S. L. Haan, J. S. Van Dyke, and Z. S. Smith, Phys. Rev. Lett. **101**, 113001 (2008).

[32] F. Mauger, A. Kamor, C. Chandre, and T. Uzer, Phys. Rev. E **85**, 066205 (2012).

[33] F. Mauger, C. Chandre, and T. Uzer, Phys. Rev. Lett. **102**, 173002 (2009).

[34] J. Tate, T. Auguste, H. G. Muller, P. Salières, P. Agostini, and L. F. DiMauro, Phys. Rev. Lett. **98**, 013901 (2007).

[35] C. Yu and L. B. Madsen, Phys. Rev. A **95**, 063407 (2017).

[36] K. Schiessl, K. L. Ishikawa, E. Persson, and J. Burgdörfer, Phys. Rev. Lett. **99**, 253903 (2007).

[37] M. V. Frolov, N. L. Manakov, and A. F. Starace, Phys. Rev. Lett. **100**, 173001 (2008).

[38] S. Micheau, Z. Chen, A.-T. Le, and C. D. Lin, Phys. Rev. A **79**, 013417 (2009).

[39] F. Mauger, C. Chandre, and T. Uzer, Phys. Rev. Lett. **104**, 043005 (2010).

[40] For intensities above 1.6×10^{14} W/cm^2, the contribution from HHG in the neutral molecule dominates over the contribution from the cation such that the secondary cutoffs become less noticeable.

[41] Y. L. Wang, S. P. Xu, Y. J. Chen, H. P. Kang, X. Y. Lai, W. Quan, X. J. Liu, X. L. Hao, W. D. Li, S. L. Hu, J. Chen, W. Becker, W. Chu, J. Yao, B. Zeng, Y. Cheng, and Z. Z. Xu, Phys. Rev. A **95**, 063415 (2017).

[42] J. Troß, X. Ren, V. Makhija, S. Mondal, V. Kumarappan, and C. A. Trallero-Herrero, Phys. Rev. A **95**, 033419 (2017).